

International Journal of Modern Physics: Conference Series
 © World Scientific Publishing Company

UNIFIED DISPERSIVE APPROACH TO $\gamma^* \rightarrow \gamma\pi\pi$ AND $\gamma\gamma \rightarrow \pi\pi$

B. Moussallam

Groupe de physique théorique, IPN bât. 100, Université Paris-Sud 11, Orsay Cedex, France

Received Day Month Year

Revised Day Month Year

A representation of the amplitude $\gamma^*(q^2) \rightarrow \gamma\pi\pi$ is proposed which combines large N_c chiral resonance Lagrangian modelling with general unitarity and analyticity properties. The amplitude is constrained from $\gamma\gamma$ scattering results and $e^+e^- \rightarrow \gamma\pi^0\pi^0$ measurements by the CMD-2 and SND collaborations. As an application, the contribution of the $\pi\pi + \gamma$ states in the HVP contribution to the muon $g-2$ are reconsidered, taking into account the effect of the strong S -wave $\pi\pi$ rescattering in a model independent way.

1. Introduction

The leading hadronic contribution to the muon $g-2$ is associated with the hadronic vacuum polarization (HVP) function, and the contribution from $\pi^+\pi^-$, proportional to the square of the pion form factor, dominates the HVP unitarity relation. This has triggered experimental efforts for measuring the pion form factor to high accuracy, in particular, via the initial-state radiation (ISR) method (see [1,2](#) and references therein). In the $e^+e^- \rightarrow \gamma\pi^+\pi^-$ cross-section, the final-state radiation (FSR) amplitude contributes in addition to the ISR. In principle, they could be separated experimentally by performing a partial-wave analysis. The FSR amplitude is also needed for computing the $\gamma\pi\pi$ contribution in the HVP unitarity relation. In practice, the FSR amplitude is often estimated using the sQED approximation, which treats the pions as point-like and non-interacting. It ignores, in particular, the influence of the strong $\pi\pi$ S -wave attraction at low energy. A modelling of this effect using a narrow σ -meson gives surprisingly large results [3](#). We discuss here an approach in which $\pi\pi$ rescattering is treated in the model independent Omnès method [4](#). It can be viewed as a generalization of classic work on the $\gamma\gamma \rightarrow \pi\pi$ amplitude [5,6,7](#) and uses $\gamma\gamma$ scattering experimental results as constraints. A further generalization to the case of two virtual photons is presented at this conference [8](#), which will be applied to the light-by-light hadronic contribution to the $g-2$.

2. Analyticity of partial-waves when $q^2 \neq 0$

The Omnès method applies to partial-wave projected amplitudes, it combines the unitarity relation and analyticity properties. We restrict ourselves here to the elastic

2 *B. Moussallam*

scattering region $s \lesssim 1 \text{ GeV}^2$ which will limit the applicability of the amplitude to virtualities $q^2 \lesssim 1 \text{ GeV}^2$. In the case of two real photons, the partial-wave amplitude is an analytic function of the $\pi\pi$ energy s , except for two cuts, the right-hand cut which lies on $[4m_\pi^2, \infty]$ and the left-hand cut on $[-\infty, 0]$. The discontinuity across the right-hand cut is given by the unitarity relations, these have exactly the same form for $\gamma\gamma$ and $\gamma^*\gamma$ amplitudes. In contrast, the left-hand cuts differ. The main issue is to properly define this cut and verify that no anomalous threshold is present.

The left-hand cut is associated with singularities of the unprojected amplitude in the crossed channels. One firstly has the pion pole in the $\gamma^*\pi^+ \rightarrow \gamma\pi^+$ amplitude (so-called Born amplitude) the $J = 0$ projection reads,

$$h_{0,++}^{Born}(s, q^2) = \frac{F_\pi^v(q^2)}{s - q^2} \left[\frac{4m_\pi^2}{\sigma_\pi(s)} L_\pi(s) - 2q^2 \right], \quad L_\pi(s) = \log \frac{1 + \sigma_\pi(s)}{1 - \sigma_\pi(s)} \quad (1)$$

with $\sigma_\pi(s) = \sqrt{1 - 4m_\pi^2/s}$. Having $q^2 \neq 0$ affects the amplitude through the pion form factor $F_\pi^v(q^2)$ but also the singularities: the Born amplitude displays a pole at $s = q^2$ in addition to a left-hand cut. Using the $q^2 + i\epsilon$ prescription moves the pole away from the right-hand cut when $q^2 > 4m_\pi^2$. Secondly, one must consider the cuts associated with $\gamma^*\pi \rightarrow n\pi \rightarrow \gamma\pi$. These processes are expected to display sharp resonance effects below 1 GeV from the vector mesons ρ, ω . We may start with a large N_c approximation, where resonances generate simple poles in $\gamma^*\pi \rightarrow \gamma\pi$ (note that scalar mesons, which violate large N_c rules are not allowed). Using a resonance chiral Lagrangian, the contributions from a vector meson exchange to the three independent invariant amplitudes read

$$\begin{aligned} A^V(s, t, q^2) &= \tilde{C}_V F_{V\pi}(q^2) \left[\frac{s - 4m_\pi^2 - 4t + q^2}{t - M_V^2} + \frac{s - 4m_\pi^2 - 4u + q^2}{u - M_V^2} \right] \\ B^V(s, t, q^2) &= \tilde{C}_V F_{V\pi}(q^2) \left[\frac{1}{2(t - M_V^2)} + \frac{1}{2(u - M_V^2)} \right] \\ C^V(s, t, q^2) &= \tilde{C}_V F_{V\pi}(q^2) \left[\frac{1}{t - M_V^2} - \frac{1}{u - M_V^2} \right] \end{aligned} \quad (2)$$

The main difference when $q^2 \neq 0$ is from the kinematics: for $\gamma\gamma \rightarrow \pi\pi$ the Mandelstam variables t, u are negative while for $\gamma^*(q^2) \rightarrow \gamma\pi\pi$ they lie in the range: $[4m_\pi^2, (\sqrt{q^2} - m_\pi)^2]$. One must then take the width of the resonance into account, and this must be done in a way consistent with the general analyticity properties for, otherwise, the Omnès method would not be applicable. This may be implemented by using a Källén-Lehmann representation, i.e. by replacing, in eq. (2)

$$\frac{1}{M_V^2 - w} \longrightarrow \widetilde{B\bar{W}}_V(w) = \frac{1}{\pi} \int_{4m_\pi^2}^{\infty} dt' \frac{\sigma(t', M_V, \Gamma_V)}{t' - w}, \quad w = t, u \quad (3)$$

The function $\widetilde{B\bar{W}}_V$ has a cut on the first Riemann sheet, while a pole appears on the second sheet. The cut structure of the partial-wave projection of the vector-exchange amplitude is illustrated on figs. 1: the left figure shows that the cut extends into the complex plane and approaches the right-hand cut. The vicinity of the right-hand cut is illustrated on the right figure. Thanks to the analytic propagator and the

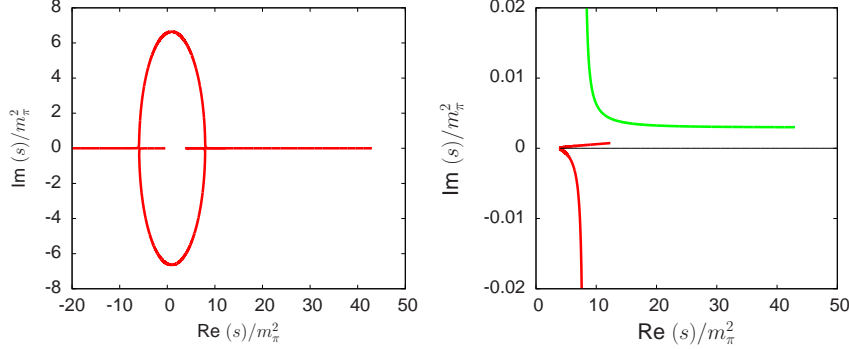


Fig. 1. Cut structure of a partial-wave projection of the vector-exchange amplitude (2).

$q^2 + i\epsilon$ prescription, no intersection actually occurs, which guarantees the absence of an anomalous threshold and the applicability of the usual Omnès method.

3. Soft photon, chiral and experimental constraints

We consider an Omnès representation for the $\gamma^* \rightarrow \gamma(\pi\pi)_I$ amplitudes based on twice-subtracted dispersion relations i.e. involving two polynomial parameters for each isospin I . These account e.g. for higher mass resonances not explicitly included and depend on q^2 . Beside the properties of analyticity and elastic unitarity, there are additional physical constraints that must be imposed. Gauge invariance imposes that the amplitudes minus the Born term must vanish in the soft photon limit⁹ which eliminates one of the parameters for each I . The helicity amplitude $H_{++}^I(s, q^2, z)$, where z is the cosine of the scattering angle in the $\pi\pi$ CMS, can be written as

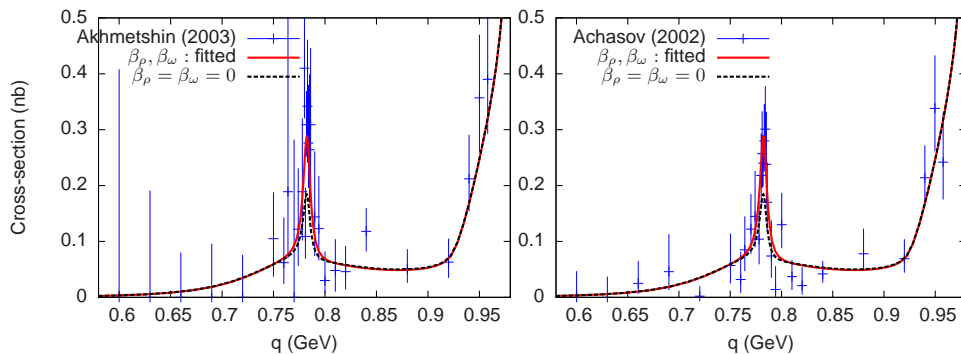
$$H_{++}^I(s, q^2, z) = H_{++}^{I, \text{Born}}(s, q^2, z) + \sum_{V=\rho, \omega} H_{++}^{I, V}(s, q^2, z) + H_{++}^{I, \text{resc}}(s, q^2, z) \quad (4)$$

The last term in eq. (4) accounts for the rescattering in the $J = 0$ partial-wave, it reads

$$H_{++}^{I, \text{resc}}(s, q^2, z) = \Omega_0^I(s) \left\{ (s - q^2) b^I(q^2) + s F_\pi^v(q^2) \left[\frac{s (J^{I, \pi}(s, q^2) - J^{I, \pi}(q^2, q^2))}{s - q^2} - q^2 \hat{J}^{I, \pi}(q^2) \right] + s \sum_{V=\rho, \omega} F_{V\pi}(q^2) \left[s J^{I, V}(s, q^2) - q^2 J^{I, V}(q^2, q^2) \right] \right\}. \quad (5)$$

Ω_0^I is the usual Omnès function and $J^{I, \pi}$, $J^{I, V}$ are the related integrals (see⁴) involving the partial-wave projections of the Born and the vector-exchange amplitudes respectively. Finally, $\hat{J}^{I, \pi} = \partial J^{I, \pi}(s, q^2) / \partial s$ at $s = q^2$. The other helicity amplitudes H_{+-} , H_{+0} are affected by rescattering from $J \geq 2$ partial-waves.

The two functions $b^0(q^2)$, $b^2(q^2)$, are constrained by chiral symmetry. In the exact chiral limit, the $\gamma^*\gamma$ amplitude for producing a π^0 pair satisfies a soft pion

4 *B. Moussallam*

 Fig. 2. Experimental results for $\sigma(e^+e^- \rightarrow \gamma\pi^0\pi^0)$ and our two parameter fit.

theorem: it vanishes at $s = 0$ for any value of q^2 . In the real world, the Adler zero moves to $s_A = O(m_\pi^2)$ and depends on q^2 . The correct chiral behaviour is enforced by matching the dispersive amplitudes for both $\pi^0\pi^0$ and $\pi^+\pi^-$ with the corresponding chiral expansion expressions ¹⁰ at $s = 0$ and small q^2 . For larger values of $q^2 \lesssim 1$ GeV² the dependence is dominated by the light vector resonances. Introducing the combinations $b^n = (-b^0 + \sqrt{2}b^2)/\sqrt{3}$ and $b^c = -(\sqrt{2}b^0 + b^2)/\sqrt{6}$ corresponding to the $\pi^0\pi^0$ and $\pi^+\pi^-$ channels, the following parametrization encodes these properties

$$b^n(q^2) = b^n(0)F_\chi(q^2) + F_R(q^2), \quad b^c(q^2) = b^c(0) + F_R(q^2) \quad (6)$$

where $F_R(q^2) = \beta_\rho(GS_\rho(q^2) - 1) + \beta_\omega(BW_\omega(q^2) - 1)$ involves the Gounaris-Sakurai and Breit-Wigner functions, and $F_\chi(q^2) = 12m_\pi^2[m_\pi^2 L_\pi^2(q^2)/q^2 + \sigma_\pi(q^2)L_\pi(q^2) + 3]$. The values of $b^n(0)$, $b^c(0)$ are determined from the polarizabilities of the π^+ and the π^0 which we take to be compatible with the chiral predictions. In the parametrization (6) we used the same resonance function for b^n and b^c i.e. we neglected the resonance contribution to b^2 . This is justified from the fact that the Omnès functions satisfy the inequality $|\Omega_2(s)| \ll |\Omega_0(s)|$ in the physically relevant region $4m_\pi^2 \leq s \leq q^2$ which suppresses the influence of b^2 . Thanks to this simplification, determining the two parameters β_ρ , β_ω from $\sigma(e^+e^- \rightarrow \gamma\pi^0\pi^0)$ allows one to predict $\sigma^{FSR}(e^+e^- \rightarrow \gamma\pi^+\pi^-)$. A combined fit to the two data sets from the SND and CMD-2 collaborations ^{11,12} gives: $\beta_\rho = 0.05 \pm 0.09$, $\beta_\omega = (-0.37 \pm 0.09) \cdot 10^{-1}$ GeV⁻² with $\chi^2/N_{dof} = 38/50$, this is illustrated in Fig.2.

4. Application to the $\pi\pi\gamma$ contributions to the muon $g - 2$

The contribution of the HVP to the muon $g - 2$ which involve two pions plus one photon can be written in terms of infrared finite cross-sections,

$$\frac{g-2}{2} \Big|_{\pi\pi\gamma} = \frac{1}{4\pi^2} \int_{4m_\pi^2}^{\infty} dq^2 K_\mu(q^2) \left(\sigma_{e^+e^- \rightarrow \pi^+\pi^-\gamma}^{sQED}(q^2) + \sum_{n,c} \hat{\sigma}_{e^+e^- \rightarrow \pi\pi\gamma}^{n,c}(q^2) \right) \quad (7)$$

where (see e.g. [13](#) for the explicit expression of the functions K_μ and η)

$$\begin{aligned}\sigma_{e^+e^- \rightarrow \pi^+\pi^-\gamma}^{sQED} &= \frac{\alpha^3}{3q^2} \sigma_\pi^3(q^2) |F_\pi^v(q^2)|^2 \times \eta(q^2) \\ \hat{\sigma}_{e^+e^- \rightarrow \pi\pi\gamma}^{c,n} &= \frac{\alpha^3}{12(q^2)^3} \int_{4m_\pi^2}^{q^2} ds (q^2 - s) \sigma_\pi(s) \int_{-1}^1 dz (|\hat{H}_{++}^{c,n}|^2 + |\hat{H}_{+-}^{c,n}|^2 + |\hat{H}_{+0}^{c,n}|^2)\end{aligned}\tag{8}$$

where $\hat{H}_{\lambda\lambda'}^n = H_{\lambda\lambda'}^{n,V+resc.}$ and $|\hat{H}_{\lambda\lambda'}^c|^2 = 2\text{Re}(H_{\lambda\lambda'}^{*Born} H_{\lambda\lambda'}^{c,V+resc.}) + |H_{\lambda\lambda'}^{c,V+resc.}|^2$.

Table 1. $\pi\pi\gamma$ contributions (central values) to the muon $g-2$ from the integration region $\sqrt{q^2} \leq 0.95$ GeV.

channel	cross-section	$(g-2)/2$
$\gamma\pi^+\pi^-$	$ H^{Born} ^2$	41.9×10^{-11}
$\gamma\pi^+\pi^-$	$H^{*Born} H^{V+resc}$	$(1.31 \pm 0.30) \times 10^{-11}$
$\gamma\pi^+\pi^-$	$ H^{V+resc} ^2$	$(0.16 \pm 0.05) \times 10^{-11}$
$\gamma\pi^0\pi^0$	$ H^{V+resc} ^2$	$(0.33 \pm 0.05) \times 10^{-11}$

The contributions to the muon $g-2$, restricting the integration range in eq. (7) to $\sqrt{q^2} \leq 0.95$ GeV, within the domain of validity of the model, are shown in table 1. As compared to previous work, we find for the contribution linear in H^{Born} a different sign than ref. [14](#), which is due to the effect of the rescattering. The results from the last two lines can be compared with ref. [3](#) who use a sigma resonance approximation: our result is smaller in magnitude by a factor of three. The table shows that the sQED contribution is largely dominant. Still, it would be of interest to be able to extend the integration range somewhat since one expects a kinematical increase of σ^{FSR} when $\sqrt{q^2} > m_\omega + m_\pi$. This would necessitate to include $J=2$ rescattering, which is easy to implement, and also account for $\pi\pi - K\bar{K}$ inelasticity.

Acknowledgements: Supported by the European Community-Research Infrastructure Integrating Activity "Study of Strongly Integrating Matter" (acronym HadronPhysics3)

References

1. D. Babusci *et al.*, *Phys.Lett.* **B720**, 336 (2013).
2. J. Lees *et al.*, *Phys.Rev.* **D86**, 032013 (2012).
3. S. Narison, *Phys.Lett.* **B568**, 231 (2003).
4. R. Omnès, *Nuovo Cim.* **8**, 316 (1958).
5. M. Gourdin and A. Martin, *Nuovo Cim.* **17**, 224 (1960).
6. D. Morgan and M. Pennington, *Phys.Lett.* **B192**, 207 (1987).
7. J. F. Donoghue and B. R. Holstein, *Phys.Rev.* **D48**, 137 (1993).
8. M. Hoferichter, G. Colangelo, M. Procura and P. Stoffer, arXiv:1309.6877, (2013).
9. F. Low, *Phys.Rev.* **110**, 974 (1958).
10. J. F. Donoghue, B. R. Holstein and Y. Lin, *Phys.Rev.* **D37**, 2423 (1988).
11. M. Achasov *et al.*, *Phys.Lett.* **B537**, 201 (2002).
12. R. Akhmetshin *et al.*, *Phys.Lett.* **B580**, 119 (2004).
13. F. Jegerlehner and A. Nyffeler, *Phys.Rept.* **477**, 1 (2009).
14. S. Dubinsky, A. Korchin, N. Merenkov, G. Pancheri and O. Shekhovtsova, *Eur.Phys.J.* **C40**, 41 (2005).